analytical chemistry

pubs.acs.org/ac Article

Dual-Signal Triple-Mode Optical Sensing Platform for Assisting in the Diagnosis of Kidney Disorders

Xiwen Ye, Dejiang Gao, Xiaowei Mu, Qiong Wu, Pinyi Ma,* and Daqian Song*

Cite This: *Anal. Chem.* 2023, 95, 4653−4661 Read Online

ACCESS | Metrics & More | Article Recommendations | Supporting Information

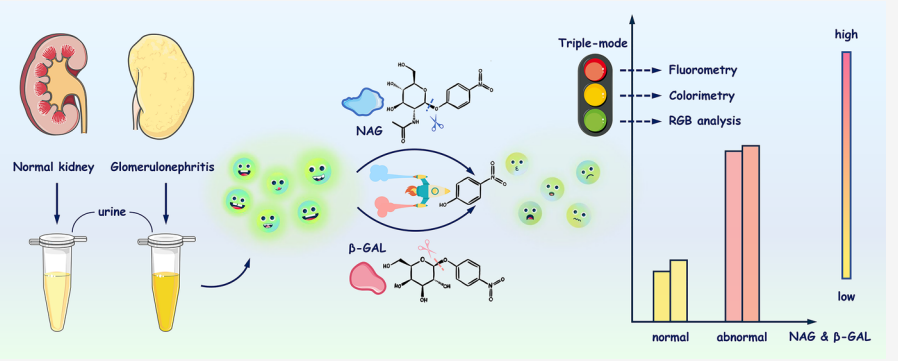

ABSTRACT: As known biomarkers of kidney diseases, *N*-acetyl-*β*-D-glucosaminidase (NAG) and *β*-galactosidase (*β*-GAL) are of great importance for the diagnosis and treatment of diseases. The feasibility of using multiplex sensing methods to simultaneously report the outcome of the two enzymes in the same sample is even more alluring. Herein, we establish a simple sensing platform for the concurrent detection of NAG and *β*-GAL using silicon nanoparticles (SiNPs) as a fluorescent indicator synthesized by a one-pot hydrothermal route. *p*-Nitrophenol (PNP), as a common enzymatic hydrolysis product of the two enzymes, led to the attenuation of fluorometric signal caused by the inner filter effect on SiNPs, the enhancement of colorimetric signal due to the increase of intensity of the characteristic absorption peak at around 400 nm with increasing reaction time, and the changes of RGB values of images obtained through a color recognition application on a smartphone. The fluorometric/colorimetric approach combined with the smartphone-assisted RGB mode was able to detect NAG and *β*-GAL with good linear response. Applying this optical sensing platform to clinical urine samples, we found that the two indicators in healthy individuals and patients (glomerulonephritis) with kidney diseases were significantly different. By expanding to other renal lesion-related specimens, this tool may show great potentials in clinical diagnosis and visual inspection.

INTRODUCTION

The kidney is a vital organ; kidney injuries leading to severe or progressive chronic kidney diseases can seriously jeopardize human health and largely increase the probability that the conditions of patients deteriorate into end-stage kidney diseases, thus improving morbidity and even mortality in patients.[1] Glomerulonephritis as a heterogeneous group of disorders presents with edema, oliguria or anuria, hypertension, proteinuria, hematuria, and renal hypofunction to a variable degree.[2] Whether a causal approach or a histopathological pattern-based approach, glomerulonephritis can be subdivided into many different categories, and all glomerulonephritis disorders can occur as periods of exacerbation.[3] Since the development of glomerulonephritis also causes other severe lesions, increases cancer risk, and even threaten life of human,[4] it is of vital importance to create new methods for the screening of incipient glomerulonephritis or seek sensitive and reliable biomarkers to stratify at-risk patients in accordance with the progressive renal function decline.

Traditional markers or measures of kidney function including albuminuria, hematuria, blood urea nitrogen, serum creatinine and urinary creatinine, urine sediment, etc.,[5,6] however, are not true markers of kidney injury or dysfunction[7] since they are neither specific nor sensitive, showing incapability of adequately responding before the considerable loss of renal function. *N*-Acetyl-*β*-D-glucosaminidase (NAG) and *β*-galactosidase (*β*-GAL) are both lysosomal hydrolases,[8,9] and they cannot be filtered through the basal glomerular membrane due to their high molecular weight (NAG of 140 kDa and *β*-GAL of 465 kDa).[7] Thus, their concentrations in

Received: November 8, 2022
Accepted: February 24, 2023
Published: March 2, 2023

https://doi.org/10.1021/acs.analchem.2c04958
Anal. Chem. 2023, 95, 4653−4661

Scheme 1. Schematic Illustration Showing the Monitoring of NAG and β-GAL by the Proposed Nanoprobe[a]

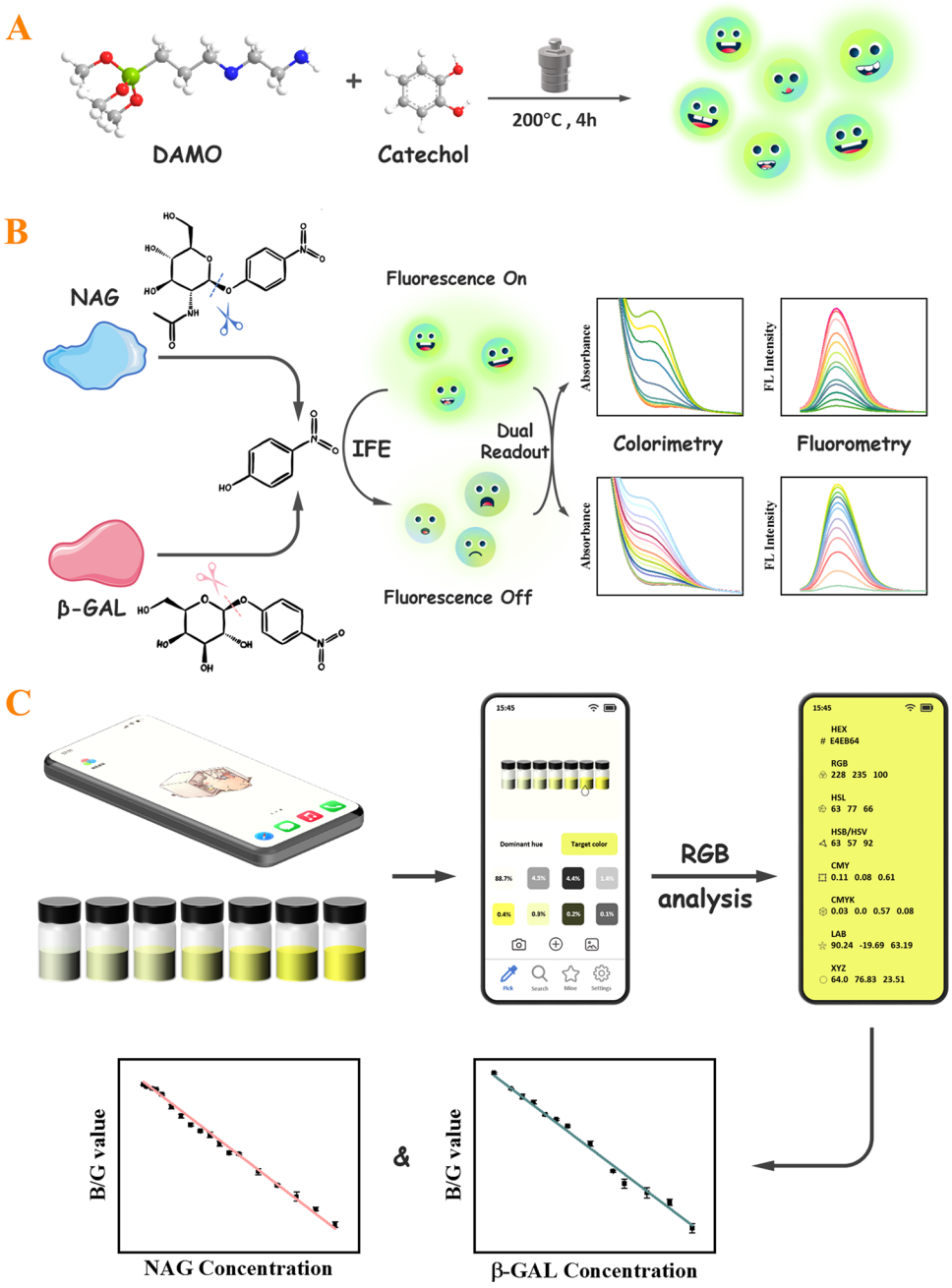

[a](A) Synthesis of the fluorescent SiNPs; (B) mechanism of monitoring NAG and β-GAL via colorimetric and fluorescent dual-mode signals; (C) RGB analysis of the smartphone-assisted method via a color recognizer APP.

the urine of healthy people are low, and elevated urinary NAG and β-GAL are exclusively caused by their secretion from damaged tubular cells when intracellular damage is determined.[7,8] NAG and β-GAL that are divided into different indicators of renal glomerular function according to the pathophysiology of renal diseases are true markers of kidney injury,[7] as they are enzymes released from damaged tubular cells and related to the development of kidney injury,[8] possessing great potentials in biomedical research and clinical chemistry. Although dozens of lysosomal enzymes have been investigated, only those possessing larger molecular weights (>80 kDa), higher tissue specificity, and high stability in biospecimens, such as NAG and β-GAL, could be considered for clinical purposes.[10] Moreover, it has already been verified that NAG is a more specific and susceptible biomarker for renal impairment.[11,12] Obviously, it is difficult to accurately identify the underlying disorders with NAG alone as a single urinary enzyme index since many clinical variables in different cases could affect NAG levels.[12] Finding correlations between NAG and other biomarkers can help for further differentiation and follow-up inspection of diseases.[12] Senescence-associated β-GAL has been reported to be upregulated to varying degrees in several renal diseases according to the literature;[13] there are also studies exploring the interactive correlation between kidney diseases and cell senescence, leading to progressive deterioration of renal function.[13,14] Certain differences in

https://doi.org/10.1021/acs.analchem.2c04958
Anal. Chem. 2023, 95, 4653−4661

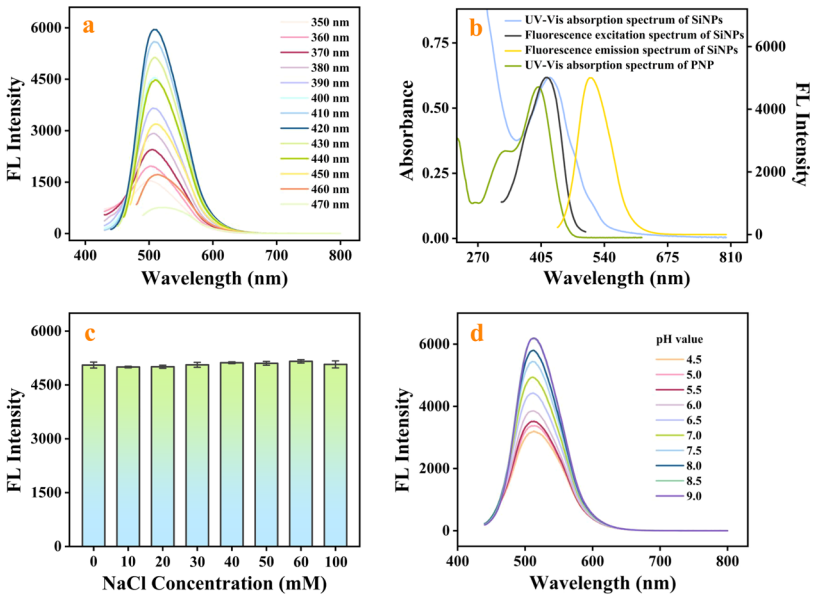

Figure 1. (a) Fluorescence emission spectra of SiNPs measured under various excitation wavelengths. (b) Fluorescence excitation and emission spectra of SiNPs and UV−vis absorption spectra of SiNPs and PNP. (c) Salt tolerance of SiNPs. (d) Fluorescence intensity of SiNPs measured at various pH values excited at 420 nm.

excretions of NAG and β-GAL in various stages of several different diseases, especially renal lesions, were enumerated in many articles as well.[10,15−17] Therefore, the simultaneous determination of NAG and β-GAL can be greatly meaningful, which contributes to ascertaining the duration and severity of lesions, discriminating between various kinds of kidney disorders, estimating the clinical outcome, and monitoring responses during the whole process from early detection to longitudinal tracking for later treatment.

Thus far, other than traditional colorimetric methods, only a few new methods, including electrochemiluminescence immunosensor[18,19] and enzyme-activated fluorescent method,[20] have been reported for NAG detection, likely due to the restriction by their complicated pretreatment procedures or high cost. Techniques for quantitatively determining the β-GAL activity have been developed, including surface-enhanced Raman scattering (SERES),[21] single photon emission computed tomography (SPECT),[22] positron emission tomography (PET),[23] bioluminescence,[24] chemiluminescence,[25] electrochemistry,[26] colorimetry,[27] and fluorometry.[28] Fluorometry has many extraordinary advantages including simple operation, high sensitivity, and real-time visualization ability.[29,30] However, techniques for concomitant, sensitive detection of both enzymes are rare. Among different fluorescent nanomaterials, silicon nanoparticles (SiNPs), as burgeoningly developed nanomaterials, inherently have superior intrinsic characteristics and many advantages[31,32] (e.g., robust fluorescence, low toxicity, storage stability, and favorable biocompatibility). For these reasons, they have been considered as propitious alternatives to organic dyes, heavy metal quantum dots, and noble metal nanoparticles.[33,34]

Herein, a smartphone-assisted multimode strategy based on fluorescent SiNPs was proposed for the simultaneous determination of NAG and β-GAL (Scheme 1). The water-dispersible, green fluorescent SiNPs were synthesized by a one-pot hydrothermal route and used as an eye-catching fluorescence indicator, since most nanodots emitted blue fluorescence. Along with the generation of p-nitrophenol (PNP), which is the common catalysis product of the two enzymes, the absorption at around 400 nm (reflects color) of the system was gradually enhanced, while the fluorescence intensity of SiNPs was incrementally restrained due to the inner filter effect (IFE). The specific recognition of enzymes to their corresponding substrates endowed the method with excellent selectivity and specificity, while the colorimetric and fluorescent dual signal guaranteed accuracy and credibility of the detection results. In addition, with the aid of a color recognizer application (APP) on a smartphone instead of complex instruments, color changes were captured, recognized, and then converted into numerical values described in the RGB mode, allowing for quantitative detection since naked eyes cannot distinguish such slight color differences.

Accordingly, a smartphone-assisted triple-channel signal sensor was fabricated and used for the simultaneous tracking of NAG and β-GAL and was further applied in the detection of human serum and urine samples. The test results of real and spiked samples could be demonstrated reciprocally by fluorescent/colorimetric dual mode, which is indicative of the reliability of the sensor, as well as its potential applicability in the field of kidney disease diagnosis. Urine samples of patients with early-stage glomerulonephritis were also tested by our methods; it was observed from our findings that urinary excretion of the two enzymes was higher in patients with glomerulonephritis than those in normal people, further proving that the combinational determination of NAG and β-GAL may help for the early clinical diagnosis of kidney disorders.

EXPERIMENTAL SECTION

Synthesis of SiNPs. Fluorescent SiNPs were prepared by a one-pot hydrothermal method reported previously[35] with slight modifications, and the details are presented in the Supplementary Information, S2.1.

Monitoring of NAG and β-GAL in Standard Solutions and Real Samples. For NAG in standard solutions, 500 μL of PB solution (200 mM, pH = 7.0), 200 μL of PNP-Nag

https://doi.org/10.1021/acs.analchem.2c04958
Anal. Chem. 2023, 95, 4653−4661

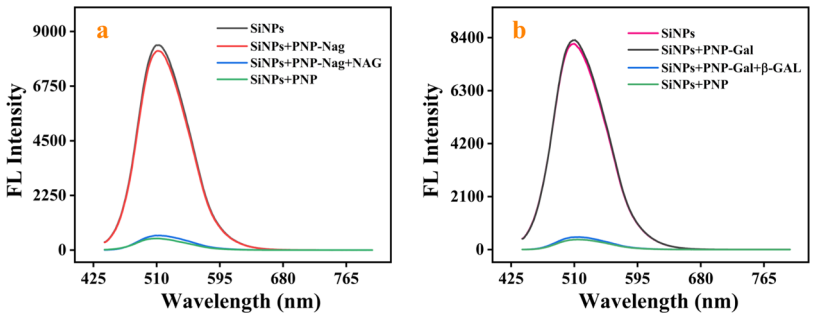

Figure 2. Fluorescence variations of SiNPs mixed with different substrates in (a) NAG-sensing system and (b) β-GAL-sensing system.

solution (5 mM), 200 μL of NAG solution at a certain concentration ranging from 0.01 U/L to 500.00 U/L, and 100 μL of SiNPs were in sequence added to a 2 mL centrifugal tube. Then, the solutions were homogeneously mixed and shaken up thoroughly in an oscillator at 37 °C for 60 min. Finally, the fluorescence spectra (excited at 420 nm) and UV−vis absorption spectra of the ultimate solutions were measured in a 1 cm quartz cuvette.

For β-GAL in standard solutions, 500 μL of PB solution (200 mM, pH = 7.4), 200 μL of PNP-Gal (7 mM), 200 μL of β-GAL solution at a certain concentration ranging from 0.01 U/L to 2000.00 U/L, and 100 μL of SiNPs were successively added to a 2 mL centrifugal tube. After that, the mixture was incubated with shaking at 37 °C in the dark for 70 min. The rest of the procedures were the same as for the measurements of NAG by the fluorescent approach and colorimetric method. All of the analytical conditions were optimized (Figures S3 and S4).

The determination of NAG and β-GAL activities in real samples can be found in the Supplementary Information, S2.2.

The ratio of the fluorescence decrease (Rfd) was calculated to indicate the efficiency of IFE, the factor associated with the measurement of the two enzymes, by the following formula

$$\text{Rfd} = \frac{F_0 - F}{F_0} \times 100\%$$

where F_0 and F represent the fluorescence emission intensity of the blank sample and the standard (or real) sample, respectively.

Fabrication of Smartphone-Assisted Platform. Since the colors of the test solutions varied with the concentrations of the enzymes, smartphone-assisted RGB assay was utilized for rapid and convenient analysis of NAG or β-Gal activity. The details of the preparation are described in the Supplementary Information, S2.3.

RESULTS AND DISCUSSION

Characterization of SiNPs. As shown in Figure S1, SiNPs were evenly dispersed spheres with an average diameter of 3.5 nm.

The Fourier transform infrared (FT-IR) spectroscopy was employed to examine the formation of SiNPs (Figure S2a), and X-ray photoelectron spectroscopy (XPS) analyses were further applied to identify their surface functional groups (Figure S2b−f). Detailed descriptions are listed in the Supplementary Information, S3.

Optical Properties of SiNPs. Optical properties of SiNPs were examined by fluorescence spectroscopy (Figure 1a) and UV−vis absorption spectroscopy (Figure 1b). The prepared SiNPs had the maximum fluorescence emission wavelength of 512 nm under an excitation wavelength of 420 nm. As the excitation wavelength was varied from 350 to 470 nm, the fluorescence emission peak was nearly unchanged, demonstrating that the size-dependent emission behavior of SiNPs was negligible. The luminescence quantum yield (QY) of SiNPs in an aqueous solution was determined to be 21.44%. The UV−vis absorption band at 422 nm may be generated as a result of the surface defect-induced trapping of excited-state energy,[36] which can lead to strong emission.

The SiNPs had excellent stability in NaCl at a high concentration of 100 mM, an indication that they have high salt tolerance (Figure 1c). Furthermore, the impact of environmental pH on the fluorescence of SiNPs was also investigated (Figure 1d). The results showed that alkaline pH enhanced the fluorescence emission intensity of SiNPs, which could be attributed to the surface charge variation caused by protonation/deprotonation.[37]

Sensing Mechanism of the System. PNP-Nag was selected as the substrate for NAG, while PNP-Gal was chosen as the β-GAL substrate. The enzymatic hydrolysis product of both NAG and β-GAL from their respective substrates is p-nitrophenol (PNP), which was involved in the reaction as an absorber. Additionally, unmodified SiNPs acted directly as a fluorophore emitting the fluorescent signal. As shown in Figure 2, the fluorescence of the system hardly fluctuated in the presence of only SiNPs and enzyme substrates, while that was significantly attenuated and quenched in the presence of SiNPs, enzymes, and their corresponding substrates or in the presence of SiNPs and PNP. The influences of enzymes, substrates, PNP, and their different combinations with SiNPs on the UV−vis absorption were also examined. As exhibited in Figure S5, both PNP-Nag and PNP-Gal showed the maximum UV−vis absorption peak at 300 nm, which had no effect on either the excitation or emission of SiNPs. By contrast, the peak for enzymatic reaction product (PNP) was shifted to around 400 nm, which greatly overlapped with the fluorescence excitation spectrum of SiNPs, therefore meeting the prerequisite for FRET and IFE (i.e., spectral overlap).[38,39] Thus, the quenching mechanism appeared to first stem from IFE or FRET.

Fluorescence resonance energy transfer (FRET) is a nonradiative energy-transfer process that occurs under the excited state of the energy donor and leads to simultaneous fluorescence quenching and lifetime shortening of fluorophores.[39,40] Generally, measuring the fluorescence lifetime is an accurate way to determine whether or not a quenching process is a dynamic process since the fluorescence decay can provide the excited-state information of the fluorophore.[41] As can be seen in Figure 3a,b, the fluorescence lifetimes of SiNPs

https://doi.org/10.1021/acs.analchem.2c04958
Anal. Chem. 2023, 95, 4653−4661

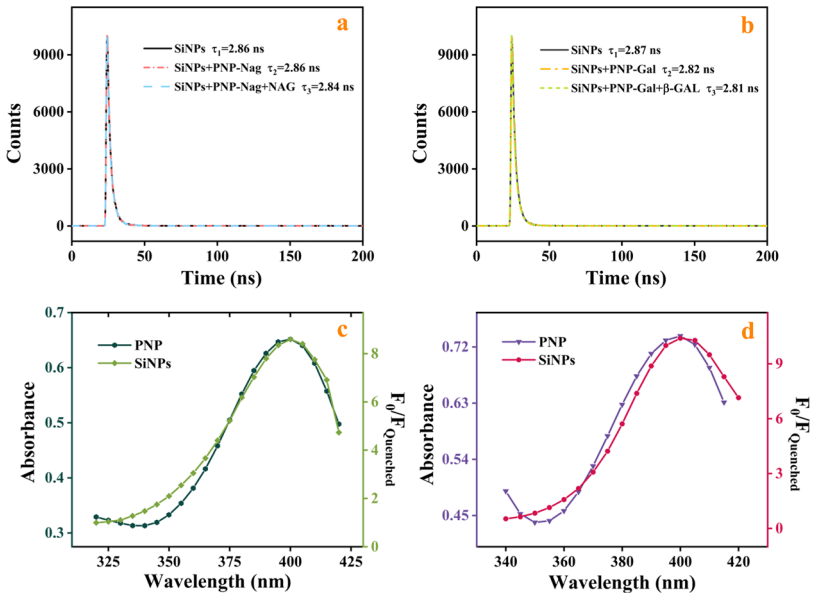

Figure 3. Fluorescent lifetime variations of SiNPs mixed with different substrates in (a) NAG-sensing system and (b) β-GAL-sensing system. Comparison between excitation wavelength-dependent fluorescence quenching behavior of SiNPs and absorption spectrum of PNP in (c) NAG-sensing system and (d) β-GAL-sensing system.

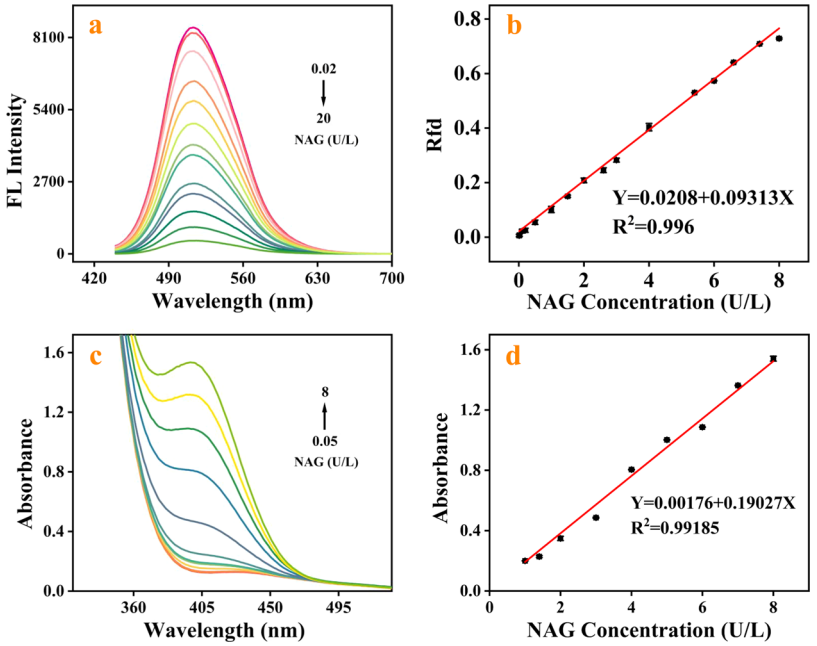

Figure 4. (a) Fluorescence spectra of SiNPs upon the addition of NAG at various concentrations. (b) Linear plot of Rfd versus NAG concentration from 0.01 to 8.00 U/L. (c) UV−vis absorption spectra of SiNPs in the presence of NAG at various concentrations. (d) Linear plot of UV−vis absorbance at 400 nm versus NAG concentration from 1 to 8 U/L.

in the two enzyme systems remained almost unchanged, indicating that the fluorescence quenching of SiNPs could not be ascribed to the perturbation of the excited state; thus, the dynamic quenching effect and FRET could be ruled out. Furthermore, FRET also depends upon the relative orientation of the donor and the transition dipoles of the acceptor, thus limiting the distance strictly to less than 10 nm,[42] whereas IFE does not need to meet this requirement. As shown in Figure S6, the electrostatic interactions in these two sensing systems were investigated, from which the zeta potential of SiNPs in the NAG-sensing system was found to be −0.482 mV (pH 7.0) and that in the β-GAL-sensing system was −0.709 mV (pH 7.4). In addition, both the mixture of SiNPs with substrates and that with substrates and enzymes were negatively charged, which is indicative of a relatively long distance between SiNPs and fluorescence quencher PNP due to electrostatic repulsion. The above evidence further proved that FRET was not part of the possible quenching mechanism. Yet, IFE stemmed from radiative energy transfer resulted in the perturbation of ground state of fluorophores, causing the fluorescence lifetime to remain unchanged after the quencher was introduced.[43,44] Moreover, different excitation wavelengths can contribute to quenching to varying degrees since the generation of IFE relies on the spectral overlap of fluorophores and absorbers. Figure

https://doi.org/10.1021/acs.analchem.2c04958
Anal. Chem. 2023, 95, 4653−4661

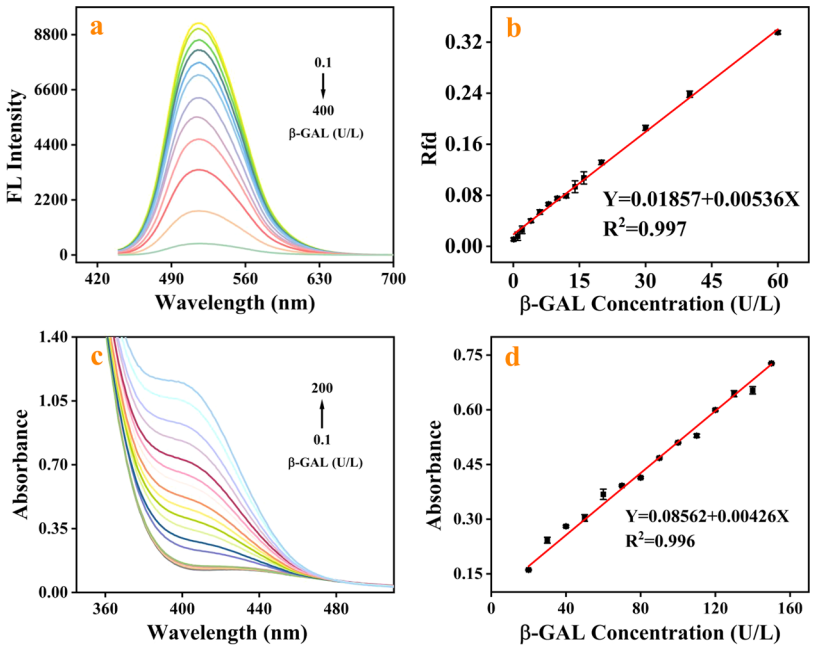

Figure 5. (a) Fluorescence spectra of SiNPs upon the addition of β-GAL at various concentrations. (b) Linear plot of Rfd versus β-GAL concentration from 0.1 to 100.0 U/L. (c) UV−vis absorption spectra of SiNPs in the presence of β-GAL at various concentrations. (d) Linear plot of UV−vis absorbance at 400 nm versus β-GAL concentration from 20 to 150 U/L.

3c,d shows that the excitation wavelength-dependent fluorescence quenching spectra of SiNPs nearly resembled the absorption spectra of PNP, thus ulteriorly confirming the occurrence of IFE mechanism. In conclusion, the sensing mechanism of the proposed fluorescent assays could be through IFE of p-nitrophenol on the fluorescence emission of SiNPs.

Fluorometric and Colorimetric Performances. Fluorescence and absorption spectral responses of the present assay to NAG at various concentrations were investigated (Figure 4a,b). As depicted in Figure 4a, the fluorescence intensity at 512 nm of SiNPs decreased gradually with increasing NAG concentration. The ratio of fluorescence decrease (Rfd) linearly correlated with NAG activity at a range of 0.01−8.00 U/L with R^2 = 0.996. The limit of detection (LOD) was 0.0086 U/L, calculated based on three times of standard deviation (3σ) of the fluorescence signals obtained by the repeated measurement of blank samples and the slope (k) of the calibration curve. The absorbance of the sensing system also obviously enhanced with the increase of NAG activity, as shown in Figure 4c. The calibration curve constructed by plotting the absorbance at 400 nm against NAG activity revealed that the absorbance was linearly correlated with NAG activity from 1 to 8 U/L, and the LOD was 0.96 U/L (Figure 4d).

Similarly, the fluorescence and absorption spectral responses of β-GAL-sensing systems are illustrated in Figure 5. The results showed that increasing β-GAL activities from 0.1 to 400.0 U/L resulted in the decrease of the maximum fluorescence intensity and the increase of Rfd value. A linear relationship was observed at a range of 0.1−100.0 U/L, according to the fluorometric method, and the LOD was calculated to be 0.084 U/L. Additionally, the absorption responses were directly proportional to β-GAL activity from 20 to 150 U/L, and the LOD was 2.3 U/L. The overall trends of fluorescence response and UV−vis absorbance with increasing concentration of either NAG or β-GAL are listed in Figure S7. The selectivity and anti-interference capacity are displayed in Figure S8.

Application in Real Human Samples. To evaluate its practicability, the present assay was employed to detect real and spiked serum samples, as well as urine samples, and the results are displayed in Tables S1−S3. All of the results listed in the tables are means of three parallel measurements ± standard deviations (SDs). Statistical significances between data obtained by fluorometric and colorimetric modes were also determined. The outcomes of the two methods were congruous and were not significantly different at a 99% confidence level, as determined by the statistical t-test. These results suggest that the proposed assay has potentials in biological detection and clinical diagnosis.

With the use of the established methods, we measured urinary NAG and β-GAL levels in a clinical range, using a cohort of patients with glomerulonephritis as an example. As listed in Tables 1 and S4, NAG and β-GAL levels in the glomerulonephritis group were elevated by several folds and were significantly different compared with those in the normal control group. This suggests that the synergism between these two parameters may be used as a new measure for clinical diagnosis and prognosis of glomerulonephritis disease. Moreover, urine collection is harmless and painless to patients and thus can be frequently conducted and allows for urinalysis to be more conveniently and easily carried out, particularly in underserved areas.

Assessment of Smartphone-Assisted Sensing Mode. As shown in Figure 6, the solution color gradually changed from pale yellow to conspicuous bright yellow, accompanied by the increase in enzyme activity. Since human eyes cannot distinguish between this subtle color change,[45] a color recognizer application installed on a smartphone was further utilized to capture a series of images and to output the corresponding RGB values for a more accurate quantitative

https://doi.org/10.1021/acs.analchem.2c04958
Anal. Chem. 2023, 95, 4653−4661

Table 1. List of NAG and β-GAL Levels by Fluorometry in Urine Samples of a Range of Patients with a Common Clinical Condition (Glomerulonephritis) and Normal People for Contrast (n = 3)[a]

Urinary enzyme	Condition	Sample number	Found (U/L)	RSD (%)	Statistical analysis[a]
NAG	Normal	1	5.21±0.24	4.70	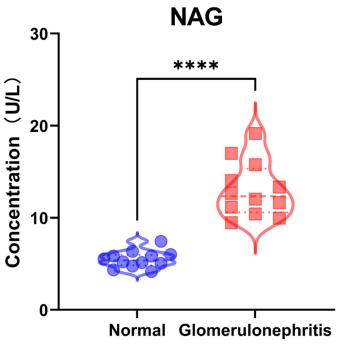
		2	7.44±0.16	2.13	
		3	5.85±0.20	3.40	
		4	4.16±0.13	3.09	
		5	4.76±0.04	0.90	
		6	6.35±0.24	3.72	
		7	5.84±0.20	3.42	
		8	5.13±0.15	2.92	
		9	4.34±0.10	2.30	
		10	5.04±0.07	1.39	
		11	5.53±0.12	2.17	
		12	6.01±0.14	2.32	
	Glomerulonephritis	13	11.65±0.10	0.89	
		14	12.02±0.53	4.40	
		15	9.47±0.30	3.19	
		16	19.15±0.75	3.92	
		17	9.96±0.43	4.31	
		18	14.04±0.41	2.91	
		19	17.00±0.39	2.31	
		20	10.42±0.40	3.84	
		21	13.34±0.38	2.85	
		22	15.76±0.32	2.03	
		23	11.15±0.51	4.57	
		24	12.65±0.22	1.74	
β-GAL	Normal	1	9.56±0.36	3.80	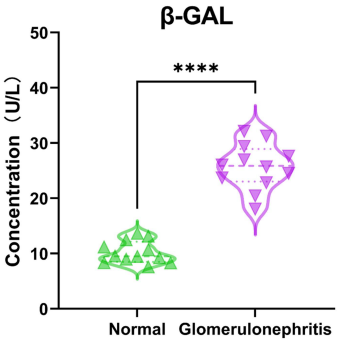
		2	10.69±0.06	0.58	
		3	8.98±0.33	3.67	
		4	7.61±0.24	3.15	
		5	9.23±0.07	0.77	
		6	13.66±0.31	2.25	
		7	11.18±0.22	1.92	
		8	8.32±0.18	2.16	
		9	13.15±0.32	2.43	
		10	9.46±0.10	1.06	
		11	12.50±0.12	0.96	
		12	8.35±0.09	1.08	
	Glomerulonephritis	13	31.25±0.54	1.74	
		14	26.97±0.84	3.10	
		15	32.12±0.58	1.81	
		16	26.04±0.40	1.53	
		17	18.06±0.49	2.72	
		18	23.71±0.47	1.99	
		19	22.82±0.44	1.93	
		20	20.45±0.38	1.86	
		21	29.37±0.52	1.77	
		22	25.70±0.66	2.57	
		23	27.62±0.42	1.52	
		24	24.51±0.70	2.86	

[a]Data analysis was performed on independent samples with equal variances (****P < 0.0001).

analysis. The blue/green values of images had a good linear relationship with NAG activity from 0.1 to 20.0 U/L, according to the regression equation B/G = −0.04575[NAG] + 0.96242 (R^2 = 0.985), and with β-GAL activity ranging from 10 to 360 U/L, according to the regression equation B/G = −0.00221[β-GAL] + 0.93633 (R^2 = 0.992). Calculated by 10σ/slope, the limit of quantification (LOQ) was 0.66 U/L for NAG and was 13.1 U/L for β-GAL. As a smartphone with mighty data reception and processing capability can be an alternative to complex instruments, this simple and portable smartphone-sensing platform may have application potential in shaping new trails for quantitative analysis.

CONCLUSIONS

In summary, we constructed a smartphone-assisted sensing platform for the simultaneous detection of NAG and β-GAL based on green fluorescent silicon nanoparticles. The enzymatic strategy is specific to the target enzymes, thus eliminating interferences by other unrelated enzymes. The generation of PNP by the two hydrolytic reactions resulted in the fluorescence quenching of SiNPs and obvious absorption of light in the visible region. Moreover, with the support of a color recognizer application on a smartphone, distinct color information could be captured and converted into blue/green value ratios that could be utilized for accurate quantitative analysis of NAG and β-GAL, which can facilitate and allow for on-site monitoring. In addition to its easy preparation and high

https://doi.org/10.1021/acs.analchem.2c04958
Anal. Chem. 2023, 95, 4653−4661

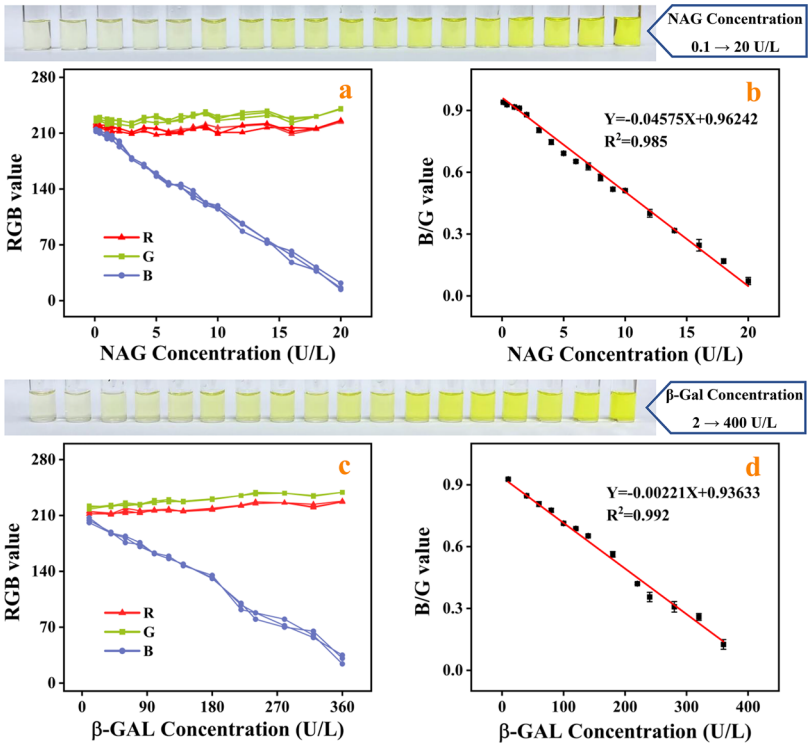

Figure 6. (a) Color changes in RGB modes of samples in NAG-sensing system. (b) Change of the blue/green value ratio of image with increasing NAG concentration from 0.1 to 20.0 U/L. (c) Color changes in RGB modes of samples in the *β*-GAL-sensing system. (d) Change of the blue/green value ratio of image with increasing *β*-GAL concentration from 10 to 360 U/L.

reliability, the established strategy was successfully applied in the analysis of human samples, e.g., in the screening for glomerulonephritis, which shows that it has high potentials in future clinical diagnosis and bioanalysis of diseases, especially for diseases related to kidney injuries.

■ ASSOCIATED CONTENT

Supporting Information

The Supporting Information is available free of charge at https://pubs.acs.org/doi/10.1021/acs.analchem.2c04958.

Additional experimental details, including reagents and instruments; experimental procedures and characterization of SiNPs; optimization of assay conditions; selectivity and anti-interference capacity of the platform; and supplementary figures and tables (PDF)

■ AUTHOR INFORMATION

Corresponding Authors

Pinyi Ma − *Jilin Province Research Center for Engineering and Technology of Spectral Analytical Instruments, College of Chemistry, Jilin University, Changchun 130012, China;* orcid.org/0000-0002-3230-4928; Email: mapinyi@jlu.edu.cn

Daqian Song − *Jilin Province Research Center for Engineering and Technology of Spectral Analytical Instruments, College of Chemistry, Jilin University, Changchun 130012, China;* orcid.org/0000-0002-4866-1292; Email: songdq@jlu.edu.cn

Authors

Xiwen Ye − *Jilin Province Research Center for Engineering and Technology of Spectral Analytical Instruments, College of Chemistry, Jilin University, Changchun 130012, China*

Dejiang Gao − *Jilin Province Research Center for Engineering and Technology of Spectral Analytical Instruments, College of Chemistry, Jilin University, Changchun 130012, China*

Xiaowei Mu − *Jilin Province Research Center for Engineering and Technology of Spectral Analytical Instruments, College of Chemistry, Jilin University, Changchun 130012, China*

Qiong Wu − *Key Laboratory of Pathobiology, Ministry of Education, Nanomedicine and Translational Research Center, China-Japan Union Hospital of Jilin University, Changchun 130033 Jilin, China*

Complete contact information is available at: https://pubs.acs.org/10.1021/acs.analchem.2c04958

Notes

The authors declare no competing financial interest.

■ ACKNOWLEDGMENTS

This work was supported by the National Natural Science Foundation of China (22074052 and 22004046) and the Natural Science Foundation of Jilin Province (YDZJ202101-ZYTS024).

■ REFERENCES

(1) Tekguc, M.; Gaal, R. C. V.; Uzel, S. G. M.; Gupta, N.; Riella, L. V.; Lewis, J. A.; Morizane, R. *Transl. Res.* **2022**, *250*, 1−17.

(2) Sethi, S.; De Vriese, A. S.; Fervenza, F. C. *Lancet* **2022**, *399*, 1646−1663.

(3) Sethi, S.; Fervenza, F. C. *Nephrol. Dial. Transplant.* **2019**, *34*, 193−199.

(4) Heaf, J. G.; Hansen, A.; Laier, G. H. *BMC Nephrol.* **2018**, *19*, 27.

(5) Liu, J. J.; Liu, S.; Wong, M. D.; Gurung, R. L.; Lim, S. C. *J. Clin. Endocr. Metab.* **2016**, *101*, 3794−3802.

(6) Vaidya, V. S.; Ozer, J. S.; Dieterle, F.; Collings, F. B.; Ramirez, V.; Troth, S.; Muniappa, N.; Thudium, D.; Gerhold, D.; Holder, D. J.; Bobadilla, N. A.; Marrer, E.; Perentes, E.; Cordier, A.; Vonderscher, J.; Maurer, G.; Goering, P. L.; Sistare, F. D.; Bonventre, J. V. *Nat. Biotechnol.* **2010**, *28*, 478−U135.
(7) Hamed, S. A. *Expert Rev. Clin. Phar.* **2017**, *10*, 993−1006.
(8) Kim, S. R.; Lee, Y. H.; Lee, S. G.; Kang, E. S.; Cha, B. S.; Kim, J. H.; Lee, B. W. *Medicine* **2016**, *95*, No. e4114.
(9) Lis, J. T.; Simon, J. A.; Sutton, C. A. *Cell* **1983**, *35*, 403−410.
(10) Xu, G. B.; Zhu, L. H.; Hong, J. M.; Cao, Y.; Xia, T. A. *J. Clin. Lab. Anal.* **1999**, *13*, 95−98.
(11) Vaidya, V. S.; Ozer, J. S.; Dieterle, F.; Collings, F. B.; Ramirez, V.; Troth, S.; Muniappa, N.; Thudium, D.; Gerhold, D.; Holder, D. J.; Bobadilla, N. A.; Marrer, E.; Perentes, E.; Cordier, A.; Vonderscher, J.; Maurer, G.; Goering, P. L.; Sistare, F. D.; Bonventre, J. V. *Nat. Biotechnol.* **2010**, *28*, 478−485.
(12) Morsby, J. J.; Smith, B. D. *Bioconjugate Chem.* **2022**, *33*, 544−554.
(13) Verzola, D.; Saio, M.; Picciotto, D.; Viazzi, F.; Russo, E.; Cipriani, L.; Carta, A.; Costigliolo, F.; Gaggero, G.; Salvidio, G.; Esposito, P.; Garibotto, G.; Poggi, L. *Am. J. Nephrol.* **2021**, *51*, 950−958.
(14) Goligorsky, M. S. *Am. J. Pathol.* **2020**, *190*, 1164−1171.
(15) Baggio, B.; Briani, G.; Cicerello, E.; Gambaro, G.; Bruttomesso, D.; Tiengo, A.; Borsatti, A.; Crepaldi, G. *Nephron* **1986**, *43*, 187−190.
(16) Price, C. P.; Foster, K. J. *Clin. Biochem.* **1979**, *12*, 231−233.
(17) Herrmann, K.; Haustein, U. F.; Bohme, H. J.; Lohrisch, I. *Brit. J. Dermatol.* **1982**, *106*, 523−528.
(18) Wang, H.; Yuan, Y.; Zhuo, Y.; Chai, Y.; Yuan, R. *Anal. Chem.* **2016**, *88*, 2258−2265.
(19) Wang, H.; Yuan, Y.; Zhuo, Y.; Chai, Y.; Yuan, R. *Anal. Chem.* **2016**, *88*, 5797−5803.
(20) Yan, F.; Tian, X.; Luan, Z.; Feng, L.; Ma, X.; James, T. D. *Chem. Commun.* **2019**, *55*, 1955−1958.
(21) Stevenson, R.; McAughtrie, S.; Senior, L.; Stokes, R. J.; McGachy, H.; Tetley, L.; Nativo, P.; Brewer, J. M.; Alexander, J.; Faulds, K.; Graham, D. *Analyst* **2013**, *138*, 6331−6336.
(22) Imbriaco, M.; Pellegrino, T.; Piscopo, V.; Petretta, M.; Ponsiglione, A.; Nappi, C.; Puglia, M.; Dell'Aversana, S.; Riccio, E.; Spinelli, L.; Pisani, A.; Cuocolo, A. *Eur. J. Nucl. Med. Mol. Imaging* **2017**, *44*, 2266−2273.
(23) Spinelli, L.; Imbriaco, M.; Nappi, C.; Nicolai, E.; Giugliano, G.; Ponsiglione, A.; Diomiaiuti, T. C.; Riccio, E.; Duro, G.; Pisani, A.; Trimarco, B.; Cuocolo, A. *Circ-Cardiovasc Imag.* **2018**, *11*, No. e007019.
(24) Mateo, C.; Palomo, J. M.; Fernandez-Lorente, G.; Guisan, J. M.; Fernandez-Lafuente, R. *Enzyme Microb. Tech.* **2007**, *40*, 1451−1463.
(25) Eilon-Shaffer, T.; Roth-Konforti, M.; Eldar-Boock, A.; Satchi-Fainaro, R.; Shabat, D. *Org. Biomol. Chem.* **2018**, *16*, 1708−1712.
(26) Tschirhart, T.; Zhou, X. Y.; Ueda, H.; Tsao, C. Y.; Kim, E.; Payne, G. F.; Bentley, W. E. *ACS Synth. Biol.* **2016**, *5*, 28−35.
(27) Hu, Q.; Ma, K.; Mei, Y.; He, M.; Kong, J.; Zhang, X. *Talanta* **2017**, *167*, 253−259.
(28) Li, X.; Qiu, W.; Li, J.; Chen, X.; Hu, Y.; Gao, Y.; Shi, D.; Li, X.; Lin, H.; Hu, Z.; Dong, G.; Sheng, C.; Jiang, B.; Xia, C.; Kim, C. Y.; Guo, Y.; Li, J. *Chem. Sci.* **2020**, *11*, 7292−7301.
(29) Ravichandiran, P.; Kaliannagounder, V. K.; Bella, A. P.; Boguszewska-Czubara, A.; Maslyk, M.; Kim, C. S.; Park, C. H.; Johnson, P. M.; Park, B. H.; Han, M. K.; Kim, A. R.; Yoo, D. J. *Anal. Chem.* **2021**, *93*, 801−811.
(30) Ravichandiran, P.; Prabakaran, D. S.; Bella, A. P.; Boguszewska-Czubara, A.; Masłyk, M.; Dineshkumar, K.; Johnson, P. M.; Park, B.-H.; Han, M.-K.; Kim, H. G.; Yoo, D. J. *ACS Sustainable Chem. Eng.* **2020**, *8*, 10947−10958.
(31) Geng, X.; Li, Z.; Hu, Y.; Liu, H.; Sun, Y.; Meng, H.; Wang, Y.; Qu, L.; Lin, Y. *ACS Appl. Mater. Interfaces* **2018**, *10*, 27979−27986.
(32) Ge, J.; Cai, R.; Yang, L.; Zhang, L.; Jiang, Y.; Yang, Y.; Cui, C.; Wan, S.; Chu, X.; Tan, W. *ACS Sustainable Chem. Eng.* **2018**, *6*, 16555−16562.
(33) Li, Q.; Luo, T. Y.; Zhou, M.; Abroshan, H.; Huang, J.; Kim, H. J.; Rosi, N. L.; Shao, Z.; Jin, R. *ACS Nano* **2016**, *10*, 8385−8393.
(34) Desai, M. L.; Basu, H.; Saha, S.; Singhal, R. K.; Kailasa, S. K. *Opt. Mater.* **2019**, *96*, 109374.
(35) Han, Y.; Chen, Y.; Feng, J.; Liu, J.; Ma, S.; Chen, X. *Anal. Chem.* **2017**, *89*, 3001−3008.
(36) Wang, X.; Cao, L.; Yang, S. T.; Lu, F.; Meziani, M. J.; Tian, L.; Sun, K. W.; Bloodgood, M. A.; Sun, Y. P. *Angew. Chem. Int. Ed.* **2010**, *49*, 5310−5314.
(37) Dong, Y.; Pang, H.; Yang, H. B.; Guo, C.; Shao, J.; Chi, Y.; Li, C. M.; Yu, T. *Angew Chem. Int. Ed.* **2013**, *52*, 7800−7804.
(38) Lakowicz, J. R. *Principles of Fluorescence Spectroscopy*, 3rd ed.; Springer: New York, 2006.
(39) Sapsford, K. E.; Berti, L.; Medintz, I. L. *Angew Chem. Int. Ed.* **2006**, *45*, 4562−4589.
(40) Stryer, L. *Annu. Rev. Biochem* **1978**, *47*, 819−846.
(41) Zhang, J.; Lu, X.; Lei, Y.; Hou, X.; Wu, P. *Nanoscale* **2017**, *9*, 15606−15611.
(42) Steinberg, I. Z. *Annu. Rev. Biochem.* **1971**, *40*, 83−114.
(43) Tanwar, A. S.; Hussain, S.; Malik, A. H.; Afroz, M. A.; Iyer, P. K. *ACS Sens.* **2016**, *1*, 1070−1077.
(44) Shang, L.; Dong, S. *Anal. Chem.* **2009**, *81*, 1465−1470.
(45) Zhou, Y.; Huang, X.; Liu, C.; Zhang, R.; Gu, X.; Guan, G.; Jiang, C.; Zhang, L.; Du, S.; Liu, B.; Han, M. Y.; Zhang, Z. *Anal. Chem.* **2016**, *88*, 6105−6109.

https://doi.org/10.1021/acs.analchem.2c04958
Anal. Chem. 2023, 95, 4653−4661